جامعة الملك عبدالله
للعلوم والتقنية
King Abdullah University of
Science and Technology

The dynamic multisite interactions between two intrinsically disordered proteins

Item Type	Article
Authors	Wu, Shaowen;Wang, Dongdong;Liu, Jin;Feng, Yitao;Weng, Jingwei;Li, Yu;Gao, Xin;Liu, Jianwei;Wang, Wenning
Citation	Wu S, Wang D, Liu J, Feng Y, Weng J, et al. (2017) The dynamic multisite interactions between two intrinsically disordered proteins. Angewandte Chemie International Edition. Available: http://dx.doi.org/10.1002/anie.201701883.
Eprint version	Post-print
DOI	10.1002/anie.201701883
Publisher	Wiley
Journal	Angewandte Chemie
Rights	This is the peer reviewed version of the following article: The dynamic multisite interactions between two intrinsically disordered proteins, which has been published in final form at http://doi.org/10.1002/anie.201701883. This article may be used for non-commercial purposes in accordance With Wiley Terms and Conditions for self-archiving.
Download date	2024-04-24 07:12:58
Link to Item	http://hdl.handle.net/10754/623649

Table of Contents

General methods

Protein expression and purification. Fragments of human 4.1G (4.1G 868-1005, 4.1G 939-1005, etc) and the human NuMA were individually cloned into a modified version of the pET32a vector or pGEX-4T-1 vector, each of the resulting proteins contained a Trx tag or GST tag in its N-termini. For NMR experiments, fragments of human 4.1G and fusion protein 4.1G 939-NuMA were individually cloned into a pET-M3C vector, each of the resulting proteins contained a His_6 tag in its N-termini. All of the mutations were created through a standard PCR-based mutagenesis method and confirmed by DNA sequencing. Recombinant proteins were expressed in *E. coli* BL21 (DE3) host cells at 16 ℃ and were purified by using Ni^{2+}-NTA or GST-agarose affinity chromatography followed by size-exclusion chromatography.

GST pull-down assay. GST or GST-tagged fusion protein (8 μM for the final concentration) were first loaded to 40-μl GSH-Sepharose 4B slurry beads in a 500-μl assay buffer containing 50 mM Tris (pH 8.0), 100 mM NaCl, 1 mM 2-Mercaptoethanol and 1 mM EDTA. The GST fusion protein loaded beads were then mixed with potential binding partners (24 μM each for the final concentration), and the mixtures were incubated for 1 h at 4 °C. After four times washing, proteins captured by affinity beads were eluted by boiling, resolved by 15% SDS–PAGE, and detected by Coomassie blue staining.

Isothermal titration calorimetry. ITC measurements were performed on an ITC200 Micro calorimeter (MicroCal) at 18 ℃. All protein samples were dissolved in a buffer containing 50 mM Tris (pH 8.0), 100 mM NaCl, and 1 mM EDTA. The titrations were carried out by injecting 40-μl aliquots of the 4.1G fragments (0.5 mM) into NuMA fragments (0.05 mM) at time intervals of 2 min to ensure that the titration peak returned to the baseline. The titration data were analyzed using the program Origin7.0 and fitted with the one-site binding model.

NMR experiments. NMR spectra of the 4.1G fragments and fusion protein 4.1G 939-NuMA were acquired at 25 ℃ on Varian Inova 600 and 800 MHz spectrometers. Sequential backbone assignments of the protein were obtained by standard heteronuclear correlation experiments, including HNCA, HNCACB, CACB(CO)NH using a ~1 mM $^{15}N/^{13}C$-labeled protein sample. NMR titration experiments were achieved using a ~0.1 mM ^{15}N-labeled 4.1G protein and ~0.05, 0.1, 0.15, 0.2 mM non-labeled NuMA protein. HSQC spectra of 4.1G939-NuMA fusion protein was acquired using a ~0.2 mM ^{15}N-labeled fusion protein. Protein samples for backbone assignment NMR experiments were in a PBS buffer of pH 6.8, with 23 mM Na_2HPO_4, 27 mM NaH_2PO_4, 1 mM EDTA, and 1mM 2-Mercaptoethanol. The protein sample for titration experiment was in a PBS buffer of pH 7.1, with 23 mM Na_2HPO_4, 27 mM NaH_2PO_4, 1 mM EDTA, and 1 mM 2-Mercaptoethanol. The fusion protein was in a PBS buffer of pH 7.4, with 23 mM Na_2HPO_4, 27 mM NaH_2PO_4, 1 mM EDTA, and 1

mM 2-Mercaptoethanol. NMR data were processed and analyzed with NMRPipe [1] and Sparky. The secondary structure propensity (SSP) scores were calculated using the Cα and Cβ chemical shifts with the method proposed by Marsh J. A. et al.[2]

Single-molecule FRET procedures

The double cysteine mutants of 4.1G were generated and purified. The 4.1G mutant proteins were labeled with the donor (Alexa Fluor 555-maleimide, Thermo Fisher Scientific Inc., MA, U.S.), and acceptor (Alexa Fluor 647-maleimide, Thermo Fisher Scientific Inc., MA, U.S.) by following the vendor provided protocol. The unreacted dye was separated from the labeled protein by using size exclusion chromatography (SEC). We cleaned the glass coverslip and drilled glass slide by sonicating them in water and ethanol three times respectively, then etched them in plasma cleaner (PDC-002, Harrick Plasma Inc., NY, U.S) for 5 min to destroy the residual dusts further. Then we stuck the coverslip on the bottom of the drilled glass slide to make a flow cell. We added about 100 μl 0.1 mg/ml poly-lysine-PEG-NTA (PLL(20)-g[3.5]-PEG(2)-NTA, SuSoS AG Inc., Switzerland) solution to the flow cell and incubated it for 20 min in order to put a layer of PEG on the coverslip surface and passivate it. After we washed the flow cell with buffer thoroughly, we added 0.1 M $NiCl_2$ solution to introduce Ni^{2+} to the NTA. After 20 min incubation and complete wash, we added 1 nM labeled protein solution to the flow cell in order to tether the protein down to the glass surface upon the binding between the His-tag of 4.1G and the NTA group on the PEG layer. To examine the non-specific binding of molecules to the glass, we performed control experiment without adding $NiCl_2$ solution. We observed very few fluorescent spots on the coverslip that is less than 6% of the number of fluorescent spots in the presence of $NiCl_2$. Such small portion of non-specific binding suggests that its effect is negligible.

The single molecule FRET images were taken by using a home-built wide-field fluorescence imaging system with an exposure time of 100 ms. In the titration experiment, one thousand-fold molar excess of NuMA was used. The smFRET time trace was extracted from the image by using iSMS software[3] and the statistical histogram of FRET was fitted to the sum of two Gaussian functions by using Matlab (Mathworks Inc., MA, U.S) program. The detailed methods refer to our previous work.[4]

Calculation of inter-dye distance

To make a direct comparison between smFRET and simulation, the FRET efficiency *ET* was converted to the donor-acceptor distance *r* according to:

$$\mathrm{r} = \left(\frac{1-ET}{ET}\right)^{1/6} R_0 \qquad (1)$$

For Alexa555 and Alexa647, the effective Förster radius R_0 was set to 51 Å. The MD simulation systems did not explicitly include the fluorophores since the large size of the dye molecules would significantly increase the computational costs. Therefore, we used the available volume (AV) method [5] to calculate the inter-dye distance based on MD snapshots. This method uses a simple geometrical algorithm assuming that all

dye positions are equally probable and there are no interactions between the dyes and the protein. The python script of AV method written by K. Walczewska-Szewc et al.[5b] was employed here to calculate the inter-dye distance. The distance distributions of smFRET measurement have a systematic deviation from those of the MD simulations (Figure 4b&c). Such discrepancy could be caused by the errors from both experiment and simulation. From the simulation side, sampling could not be perfect although the enhanced sampling algorithm REMD method was employed. And since we did not explicitly include dye molecules in the simulation, AV method could also introduce errors. From the experimental side, errors include the uncertainty in FRET efficiency measurements, and the variations of effective Förster radius R_0 due to anisotropic tumbling of the donor and acceptor fluorophores, or changes in the donor quantum yield. R_0 is proportional to the sixth roots of the orientation factor κ^2 and the donor quantum yield Q_D. The orientation factor κ^2, which is assigned a value of 0.67 based on an assumption of perfect isotropic tumbling can in fact sample a wide range of values.

Shot noise analysis

Shot noise and protein conformational motions are the main factors that contribute to the width of FRET efficiency distribution. The upper bound of shot noise variance can be calculated by: [7]

$$\sigma_{shot}^2 = \frac{\langle ET\rangle(1-\langle ET\rangle)}{\langle N\rangle} \quad (2)$$

where <*ET*> is the mean value of FRET efficiencies and <*N*> is the mean number of detected photons of all the events that are used to build the smFRET efficiency histogram. Since the electron multiplication process of the EMCCD camera that was employed in our measurement to detect the fluorescence signal of single molecules added extra multiplicative noise to the shot noise, the variance of overall shot noise is:

$$\sigma_{all-shot}^2 = 2\sigma_{shot}^2 \quad (3)$$

The subtraction of overall shot noise $\sigma_{all-shot}^2$ from the efficiency histogram variance σ_{ET}^2 gives the non-shot noise variance of the histogram $\sigma_{non-shot}^2$:

$$\sigma_{non-shot}^2 = \sigma_{ET}^2 - \sigma_{all-shot}^2 \quad (4)$$

We fitted the efficiency histogram with the sum of two Gaussian functions (Fig. S9) and obtained the <*ET*> and σ_{ET}^2 of both subpopulations separately. As listed in Table S2, the shot noise only contributes a small fraction of the histogram variance σ_{ET}^2. Although the donor-acceptor orientation and other experimental factors may contribute to the non-shot noise variance $\sigma_{non-shot}^2$, given the significant change of distributions upon ligand binding and the observation of FRET transitions under all conditions, it is convincible to conclude that the broad profile of FRET histograms represents the conformational heterogeneity of 4.1G.

Hidden Markov Model analysis

The HMM analysis was performed by applying the ebFRET method[6] to determine the FRET states of each FRET trajectory. The maximum number of states was set to 10. Then all the transition between different FRET states were compiled together to

construct the transition density plot (TDPs) that has the axis of initial versus final FRET efficiency.

MD simulations and data analysis. The conformational spaces of 4.1G939-1005 and its complex with NuMA1800-1825 peptide were explored using replica-exchange molecular dynamics (REMD)[8] simulations with explicit water. For the 4.1G939-1005 system, four initial structures were obtained from the structural prediction programs I-TASSER[9] and QUARK[10] and were evenly distributed in 48 different replicas for REMD simulation. The simulation was conducted using GROMACS-4.6.5 software package[11] with CHARMM27 force field[12] and the TIP3P water model. Na^+ and Cl^- ions were added to neutralize the system and conferred a salt concentration of 0.1 M. The system was first energy minimized using the steepest descent algorithm, and the added solvent was equilibrated with position restraints on the heavy atoms of the protein. The temperatures were maintained using the V-rescale method[13] with a relaxation time of 0.1 ps. We used the Parrinello-Rahman barostat[14] to keep the pressure at 1 bar with a time constant of 2 ps. The cutoff of electrostatic interactions and van der Waals interactions were both set to be 1.2 nm, and the particle mesh Ewald method[15] was used to treat electrostatic interactions. All bonds were constrained by the LINCS algorithms.[16] A total of 48 different temperatures ranging from 310-430 K were generated from the web server Temperature generator for REMD-simulations.[17] The exchange time between two adjacent replicas was 2 ps and each replica lasted for 200 ns. The average acceptance ratio was 23%. To confirm the convergence of the simulation, we checked the backbone RMSD, probabilities of secondary structure contents, the probability distributions of the inter-residue distance of 4.1G939-1005 within two independent time intervals (60-130 and 130-200 ns), which are all very similar (Fig. S11).

For the 4.1G/NuMA complex system, initial structures were chosen from the trajectory of 4.1G939-1005 simulation. The trajectory of 4.1G939-1005 simulation at 310 K was clustered using the Gromos clustering algorithm.[18] The center structures of the top 14 clusters were chosen to perform molecular docking with NuMA1800-1825 peptide using the online HADDOCK server,[19] and residues involved in the interaction were derived from previous site-directed mutagenesis experiments.[20] 28 initial conformations of 4.1G/NuMA complex obtained from the docking results were evenly distributed in 56 different replicas for REMD simulation and other details were the same as those for isolated 4.1G939-1005 system. The average acceptance ratio was 25%. The results were also subjected to convergence tests (Fig. S12)

The last 140 ns of trajectories at 310 K were used for analysis. All secondary structure analyses of the simulation trajectories were performed using the DSSP program[21]. Chemical shift prediction based on REMD simulations was performed using the SHIFTX2 software.[22] Secondary chemical shift $\Delta\delta$, such as $\Delta\delta$ of Cα ($\Delta\delta_{C\alpha}$), is defined as $\Delta\delta_{C\alpha} = \delta C\alpha^{exp/simu} - \delta C\alpha^{random}$. When calculating the contact probability map, two residues within 0.3 nm were regarded as a contact, and the contacts between

residue *i* and *i*+1 as well as those between residue *i* and *i*+2 were not counted because the probabilities of these contacts are always close to 1 no matter what the secondary structure is.

Cluster analysis

Cluster analysis was conducted using the Gromos algorithm with a backbone RMSD cut-off of 0.3 nm. First, the RMSD of backbone atoms between all pairs of structures were calculated. For each structure, the number of other structures with RMSD ≤ 0.3 nm was calculated. The structure with highest number of neighbors was taken as the center of a cluster. The structures of this cluster were then eliminated from the pool of the structures. This procedure was repeated until the pool of structures was empty, and a series of non-overlapping clusters were obtained.

To examine the dependence on clustering methods, we compared another two clustering methods with the Gromos algorithm, i.e. the quality threshold (QT) algorithm (*Genome Res* **1999**, *9*, 1106-1115.) implemented in the Visual Molecular Dynamics (VMD) package, and the single linkage (SL) algorithm (*The interpretation of analytical chemical data by the use of cluster analysis*, Wiley, **1983**.) implemented also in Gromacs package. Though the algorithms adopt the same cutoff value (0.3 nm for backbone RMSD) to decide whether a structure is assigned to a cluster, the Gromos algorithm compares the cutoff with the RMSD between the structure and the center structure of the cluster, whereas the QT algorithm compares the cutoff with the maximum of the RMSDs between the structure and all members of the cluster, which often leads to smaller clusters. The SL algorithm adds the structure to the cluster when the RMSD to any member of the cluster is less than the cutoff, and often leads to larger clusters. The top 15 clusters extracted by the Gromos algorithm show a clear one-to-one correspondence relationship with the top clusters extracted by the other two algorithms, including very similar center structures (RMSD < 0.2 nm) and comparable populations (Table S2), indicating that the representative structures of 4.1G939-1005 in Fig. 2d is generally insensitive to the cluster algorithm selected. Case is very similar for the 4.1G939-1005/NuMA1800-1825 complex.

Supplementary Figure 1

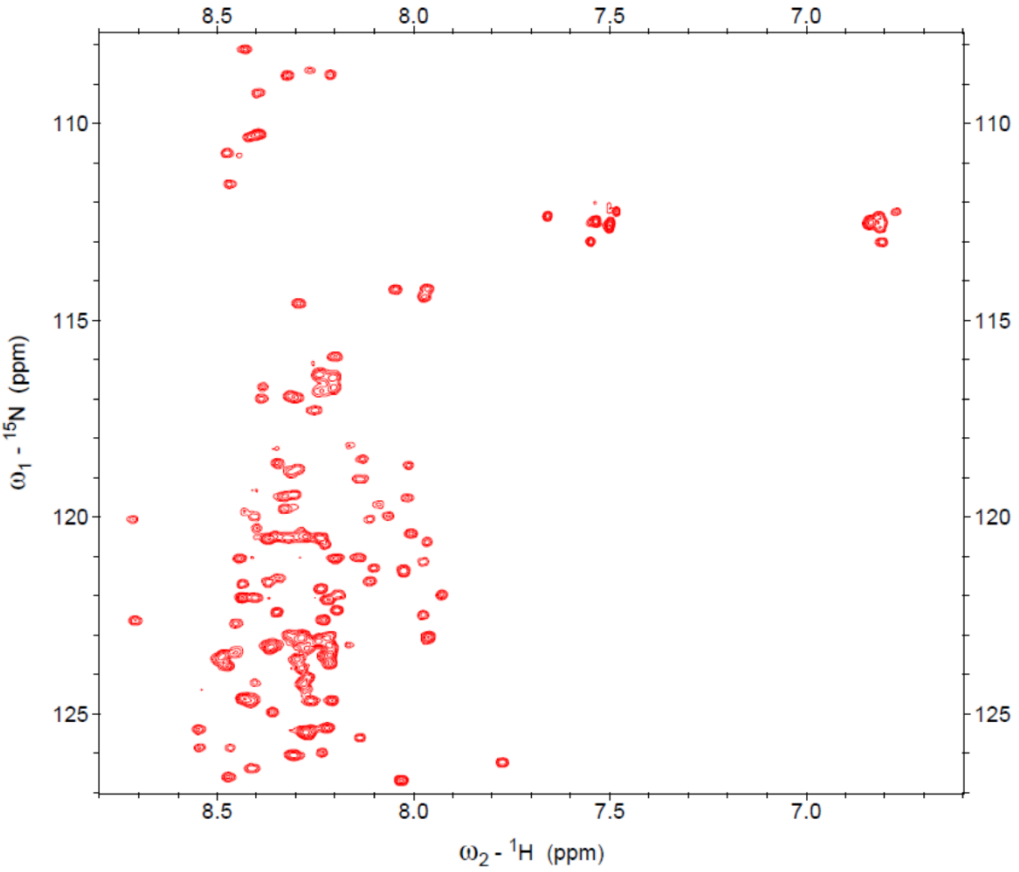

Figure S1. NMR ^{1}H-^{15}N HSQC spectrum of 4.1G868-1005, showing that this fragment is also intrinsically disordered.

Supplementary Figure 2

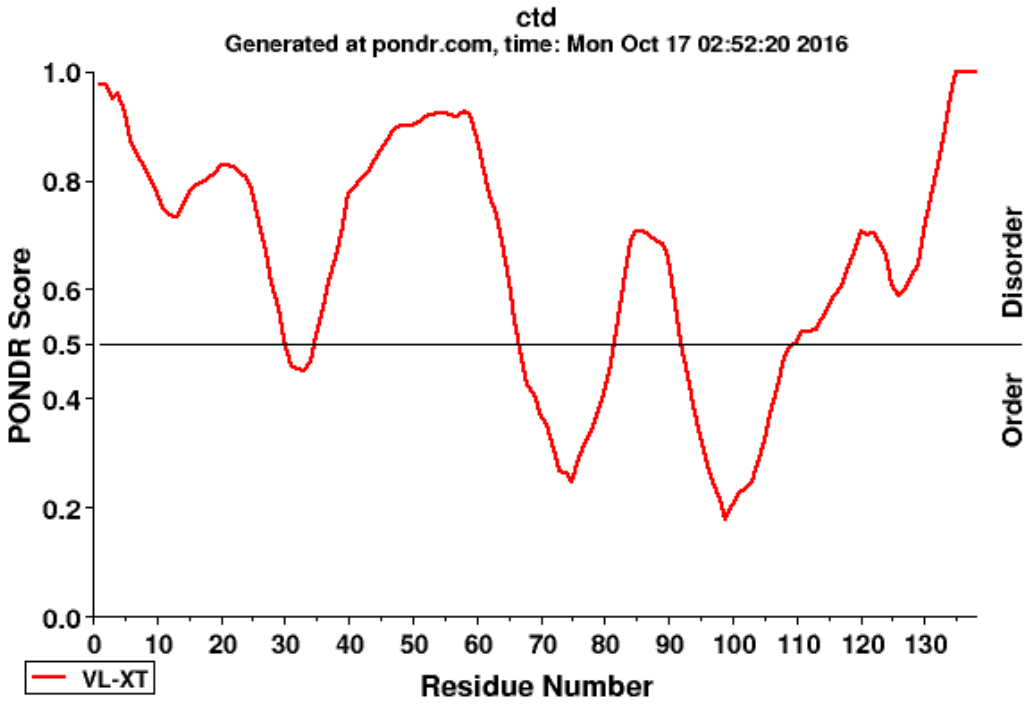

Figure S2. The predicted structural disorder based on sequence of 4.1G868-1005 by using PONDR.[23]

Supplementary Figure 3

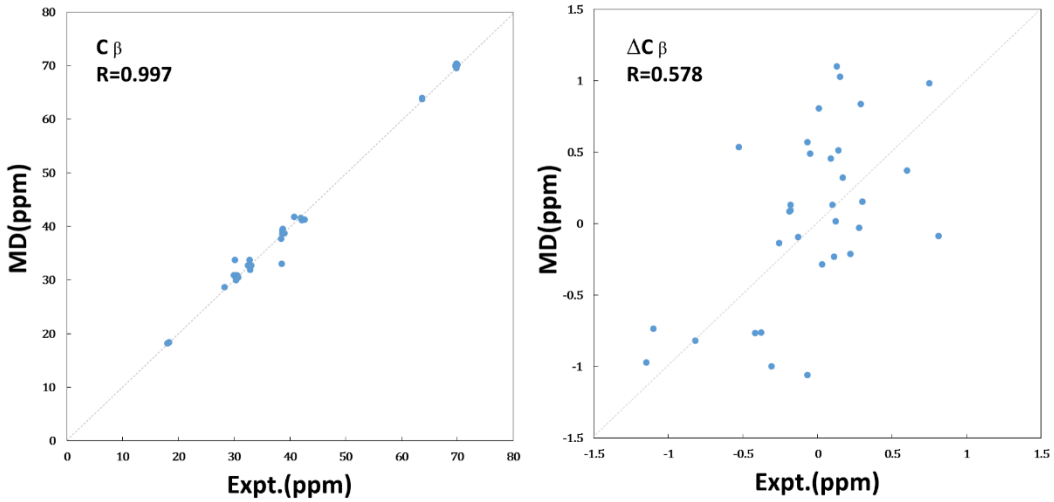

Figure S3. Agreement between the calculated and experimental Cβ chemical shifts (left) and secondary chemical shifts (right).

Supplementary Figure 4

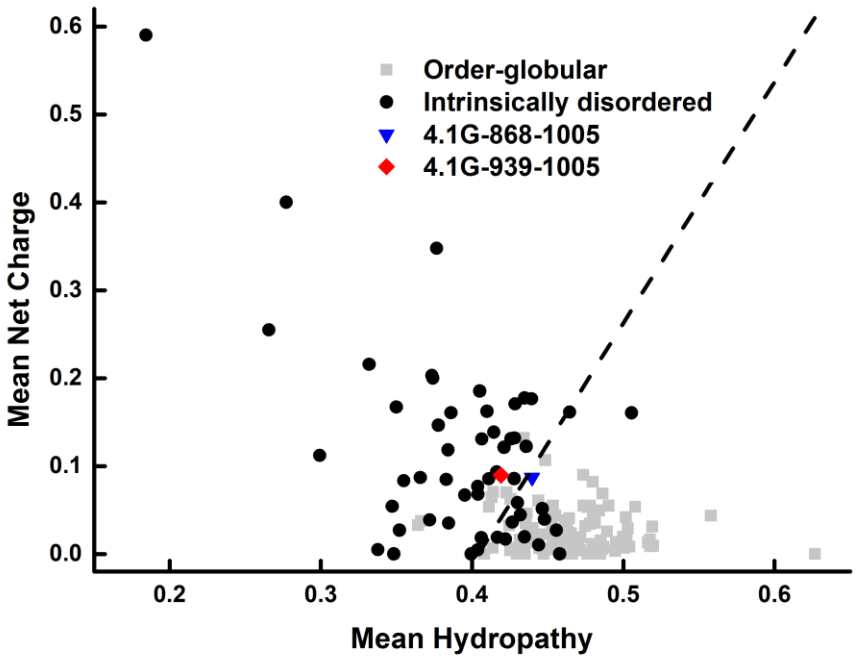

Fig. S4. **Charge hydropathy ratio for IDPs.** The dotted line represents an empirically determined charge/hydropathy relationship that distinguishes most order-globular and intrinsically disordered proteins.

Supplementary Figure 5

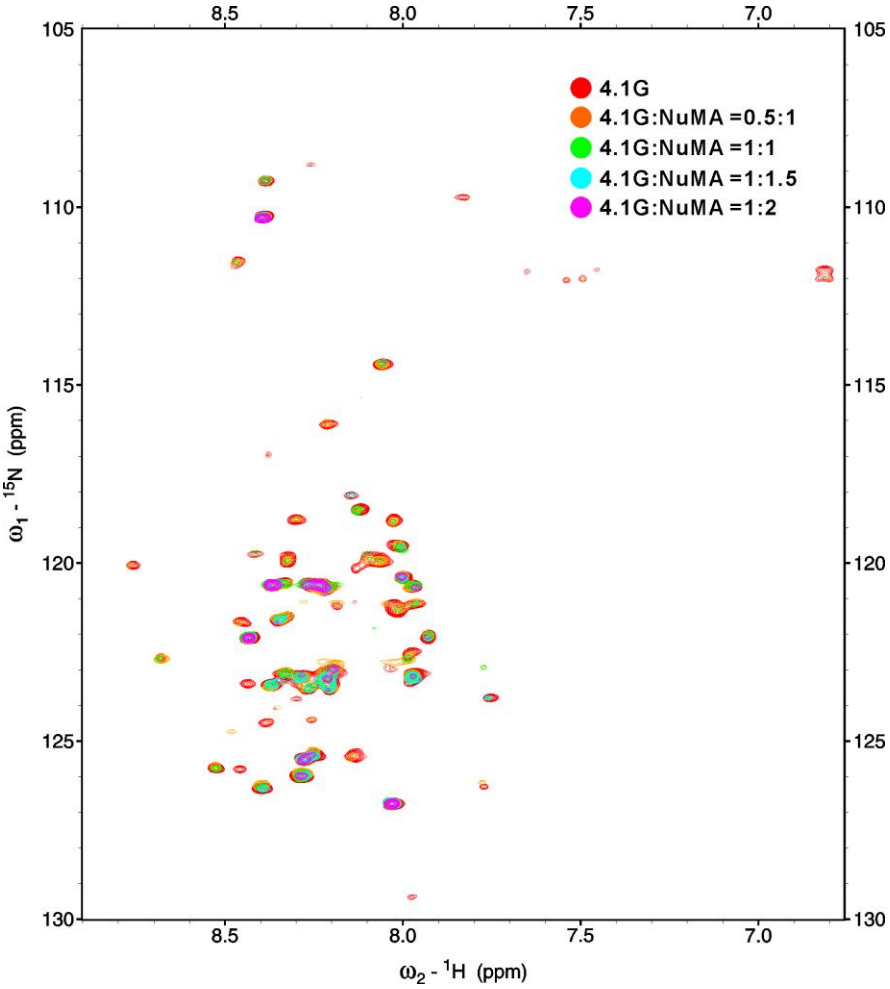

Figure S5. ^{1}H-^{15}N HSQC spectra of 4.1G939-1005 (red) and 4.1G939-1005 titrated with various molar ratios of NuMA1800-1825 (orang, green, cyan and magenta).

Supplementary Figure 6

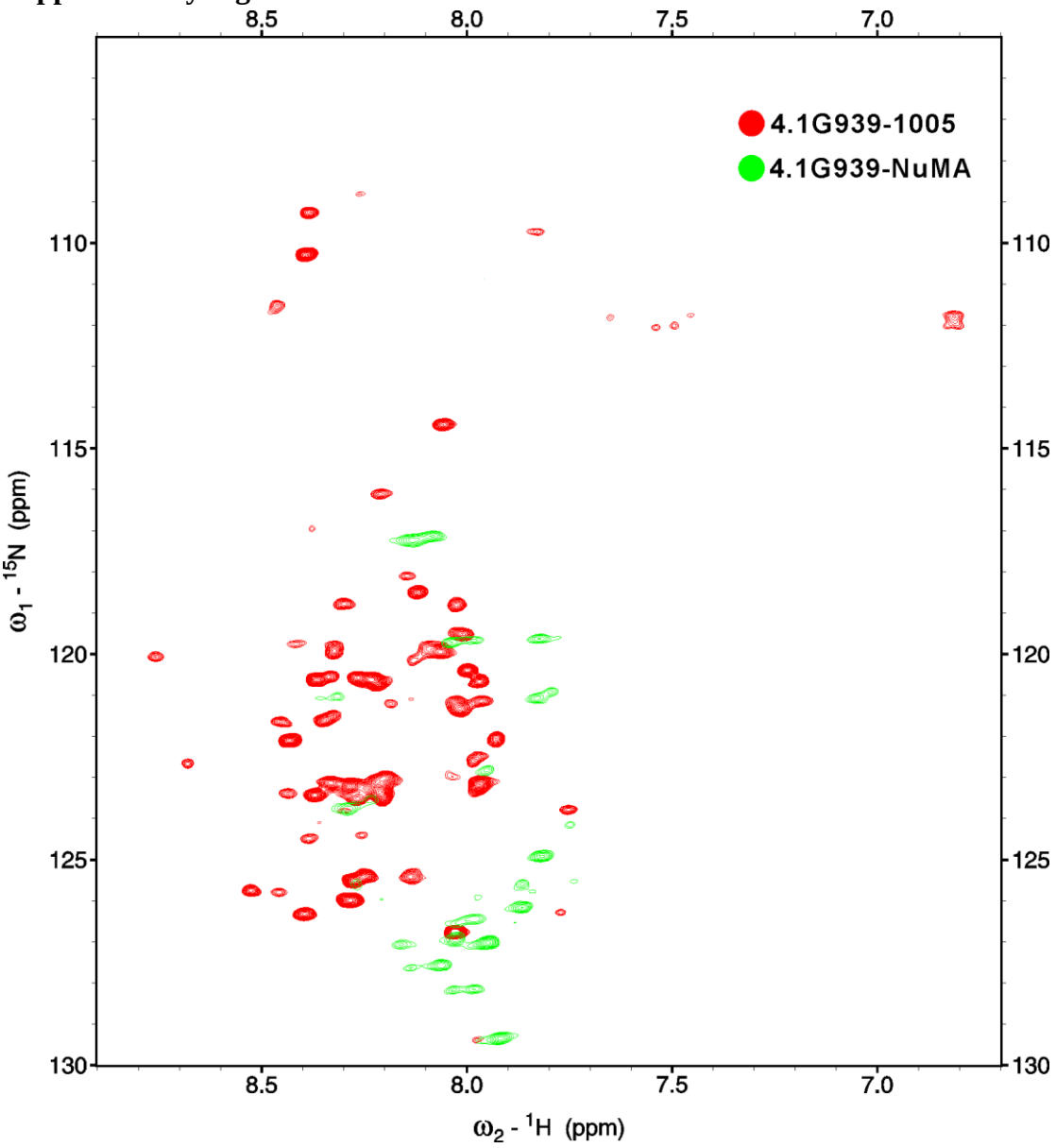

Figure S6. ^{1}H-^{15}N HSQC spectra of fusion protein 4.1G939-NuMA (green) superimposed with that of 4.1G939-1005 (red).

Supplementary Figure 7

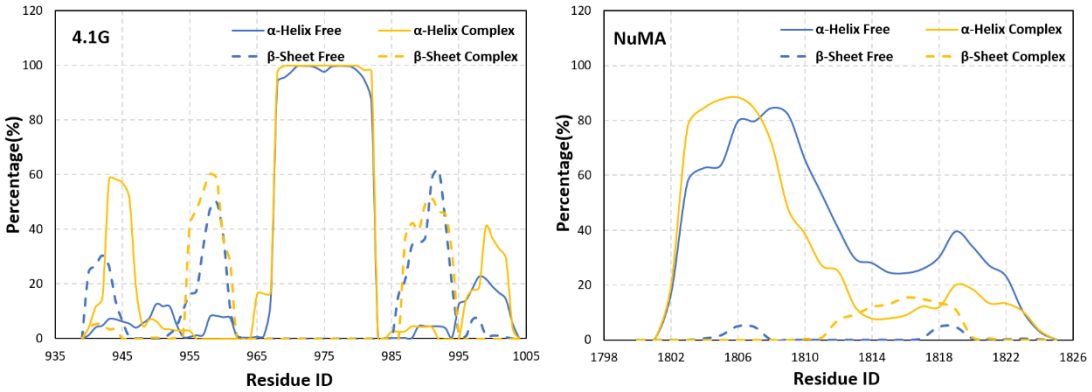

Figure S7. Calculated secondary structure contents in 4.1G939-1005 and NuMA peptide based on REMD simulation trajectories.

Supplementary Figure 8

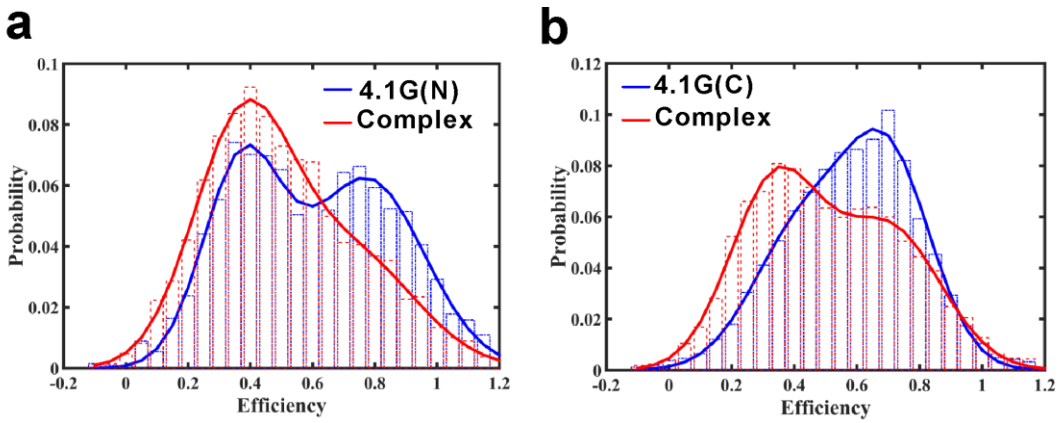

Figure S8. FRET efficiency histograms for the two labeling schemes of both 4.1G and 4.1G/NuMA complex plotting each time bin of the photon bursts. Blue: 4.1G939-1005; Red: 4.1G939-1005/NuMA.

Supplementary Figure 9

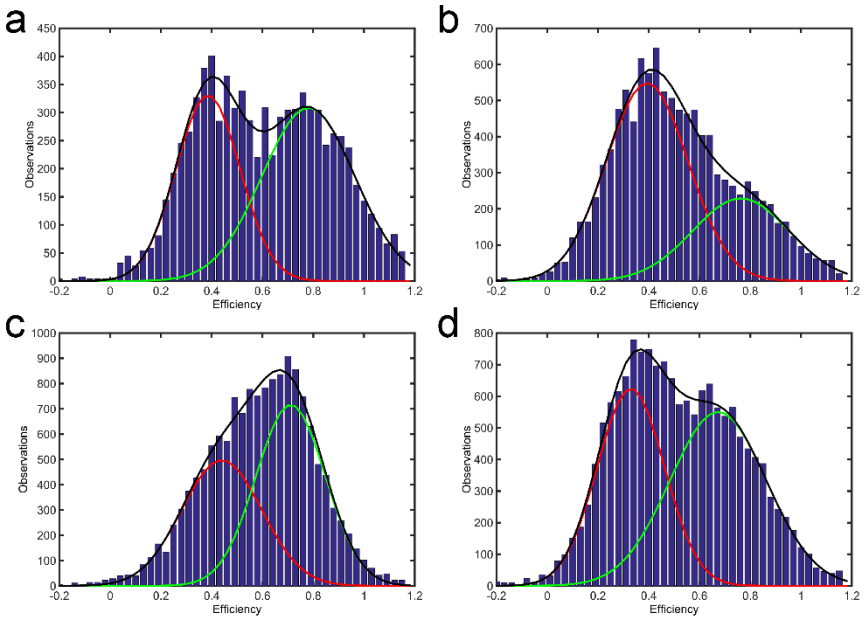

Figure S9. The smFRET efficiency histogram fitted with the sum of two Gaussian functions. (a) 4.1G(N). (b) 4.1G(N)/NuMA. (c) 4.1G(C). (d) 4.1G(C)/NuMA. Those fit values have been used to calculate shot noise variance and histogram variance.

Supplementary Figure 10

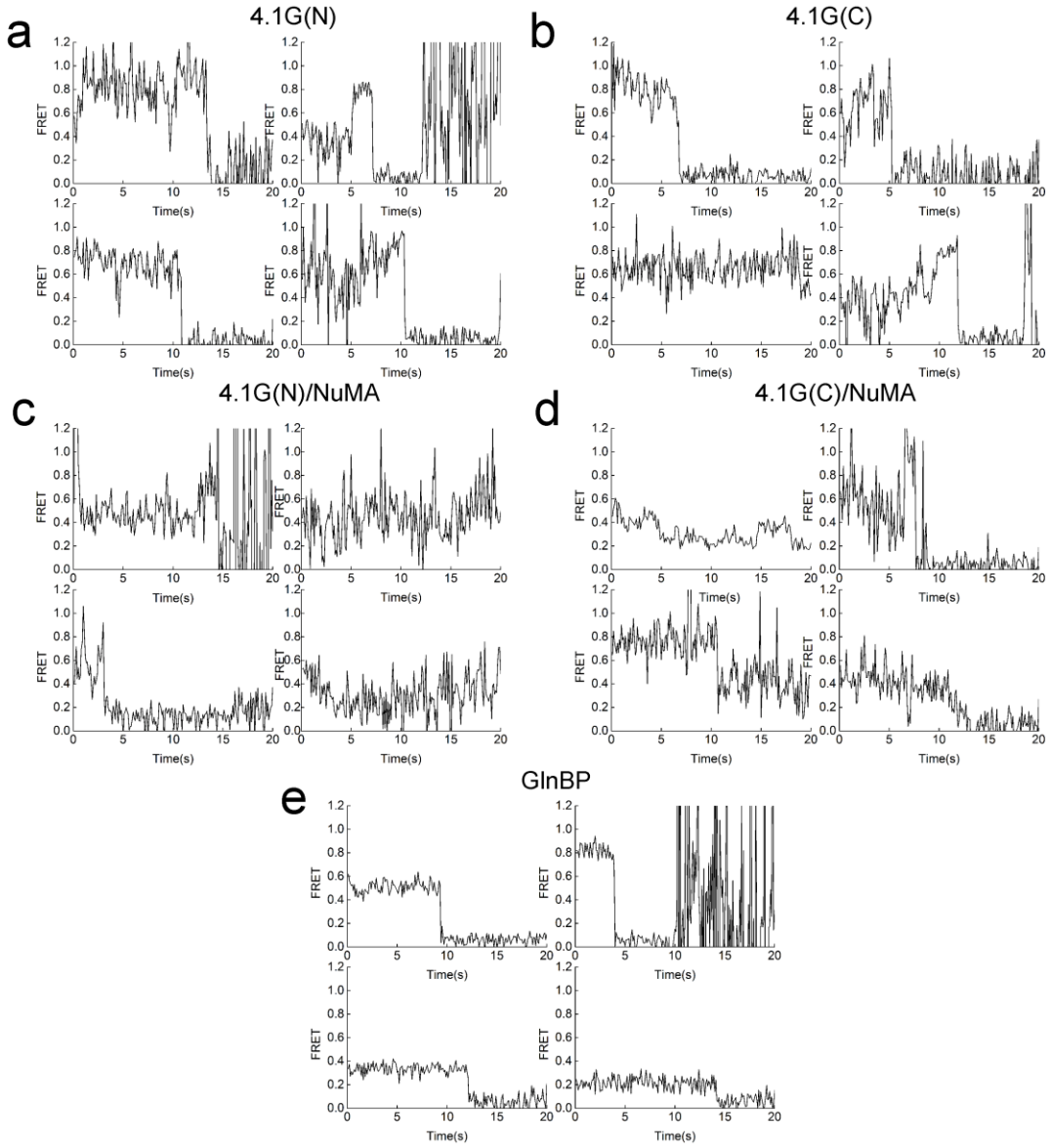

Figure S10. Example smFRET time traces of 4.1G(N) (a), 4.1G(C) (b), 4.1G(N)+NuMA (c), 4.1G(C)+NuMA (d) and GlnBP (e). GlnBP is a well-structured protein, the FRET time trace of which is distinct from those of intrinsically disordered 4.1G939-1005.

Supplementary Figure 11

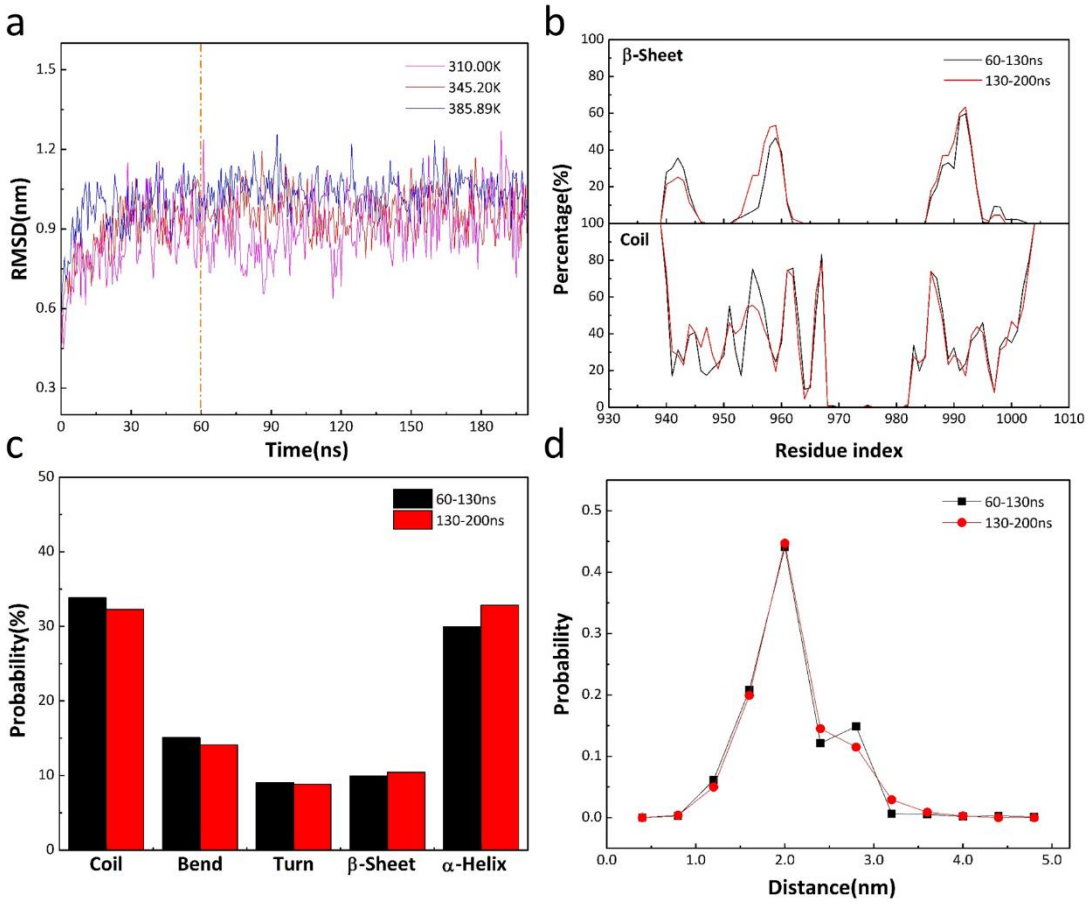

Figure S11. **Convergence of the REMD simulation of 4.1G939-1005.** Convergence of the REMD run for 4.1G939-1005 at 310K. (a) RMSD of all backbone atoms evolution at 3 temperatures. (b) The percentages of β-sheet and coil as a function of residues at two time intervals (60-130ns and 130-200ns). (c) Probability of main secondary structures. (d) The probability density function of the distance between residue 939 and residue 982.

Supplementary Figure 12

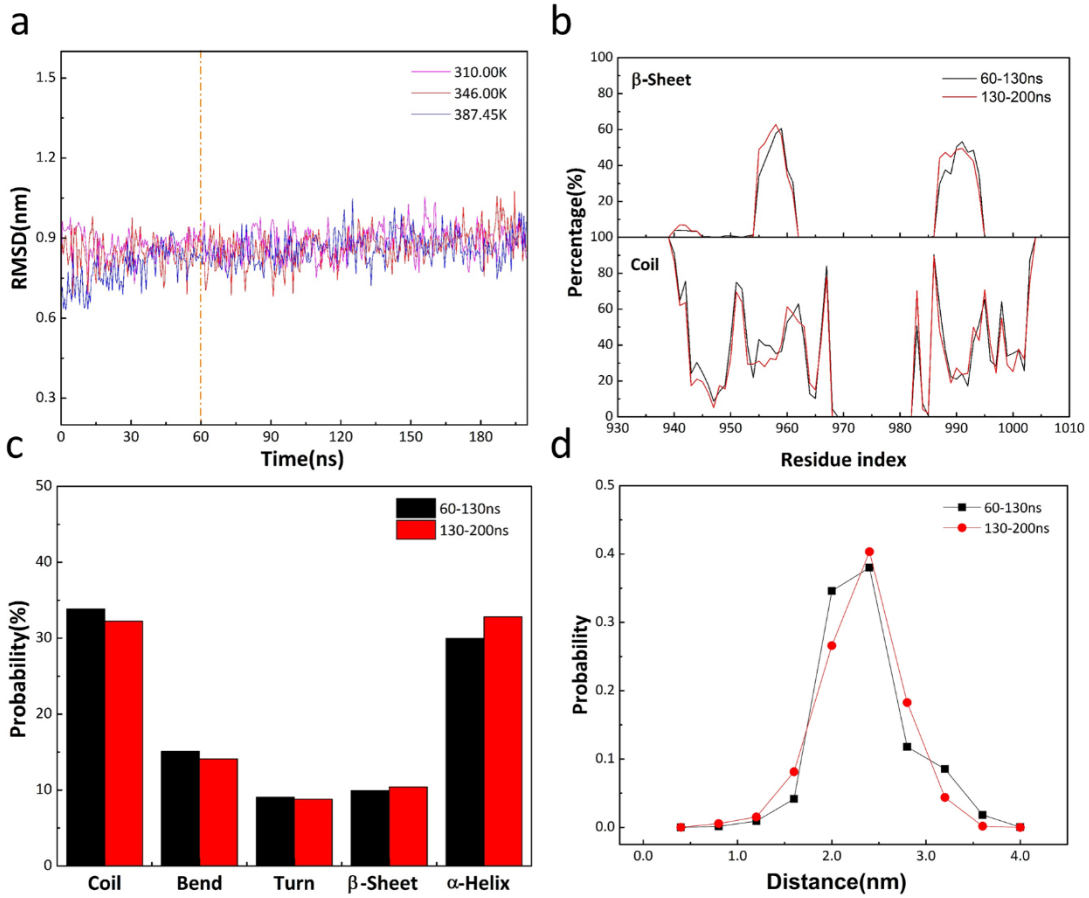

Figure S12. **Convergence of the REMD simulation for 4.1G-NuMA complex.** (a) RMSD of all backbone atoms evolution at 3 temperatures. (b) The percentages of β-sheet and coil as a function of residues at two intervals (60-130ns and 130-200ns). (c) Probability of main secondary structures. (d) The probability density function of the distance between residue 939 and residue 982.

Table S1. The most similar counterparts of 4.1G/NuMA complex in the structure ensemble of 4.1G939-1005 with minimum backbone RMSDs.

Cluster No.[a]	Cluster No.[b]	RMSD[c] (nm)	Cluster No.[a]	Cluster No.[b]	RMSD[c] (nm)	Cluster No.[a]	Cluster No.[b]	RMSD[c] (nm)
1	1	0.74	34	95	0.67	67	94	0.61
2	1	0.44	35	39	0.66	68	69	0.55
3	39	0.63	36	11	0.45	69	82	0.59
4	94	0.65	37	50	0.60	70	95	0.63
5	20	0.66	38	106	0.71	71	74	0.57
6	89	0.50	39	87	0.44	72	90	0.63
7	58	0.58	40	25	0.67	73	45	0.74
8	80	0.58	41	52	0.71	74	48	0.64
9	85	0.62	42	25	0.71	75	39	0.65
10	52	0.51	43	94	0.51	76	39	0.57
11	39	0.52	44	97	0.43	77	14	0.55
12	58	0.54	45	10	0.65	78	84	0.47
13	10	0.63	46	103	0.48	79	44	0.76
14	4	0.42	47	39	0.55	80	69	0.53
15	11	0.47	48	105	0.54	81	106	0.68
16	87	0.53	49	106	0.52	82	11	0.47
17	94	0.60	50	39	0.61	83	11	0.69
18	39	0.65	51	52	0.57	84	90	0.71
19	17	0.47	52	58	0.61	85	1	0.45
20	1	0.48	53	17	0.75	86	45	0.58
21	1	0.47	54	52	0.49	87	17	0.86
22	73	0.73	55	54	0.80	88	36	0.73
23	14	0.54	56	39	0.64	89	46	0.64
24	44	0.70	57	44	0.81	90	52	0.59
25	85	0.57	58	68	0.47	91	10	0.64
26	68	0.44	59	58	0.49	92	106	0.64
27	52	0.52	60	37	0.60	93	1	0.47
28	58	0.60	61	60	0.72	94	74	0.74
29	52	0.57	62	52	0.56	95	106	0.53
30	106	0.53	63	69	0.50	96	103	0.68
31	1	0.65	64	93	0.64	97	11	0.45
32	74	0.67	65	44	0.71	98	106	0.51
33	37	0.62	66	104	0.64			

[a] The cluster number of 4.1G/NuMA complex; [b] The cluster number of 4.1G939-1005 that has minimum backbone RMSD with the corresponding cluster of the complex. [c] The value of the minimum RMSDs.

Table S2. The contribution of shot noise to the histogram variance

System	Population-1			Population-2		
	σ_{ET}^2	$\sigma_{all-shot}^2$	$\sigma_{non-shot}^2$	σ_{ET}^2	$\sigma_{all-shot}^2$	$\sigma_{non-shot}^2$
4.1G(N)	0.016	0.0034	0.013	0.033	0.0024	0.031
4.1G(N)/NuMA	0.026	0.0042	0.022	0.036	0.0031	0.033
4.1G(C)	0.025	0.0033	0.022	0.019	0.0028	0.016
4.1G(C)/NuMA	0.017	0.0019	0.015	0.036	0.0019	0.034

Table S3. Comparison of the clustering results of the 4.1G939-1005 structures obtained by the Gromos, the quality threshold (QT), and the single linkage (SL) clustering algorithms.

Gromos[a] cluster No.	QT[b] cluster No.	SL[c] cluster No.	Gromos population (%)	QT population (%)	SL population (%)	Gromos-QT RMSD[d] (nm)	Gromos-SL RMSD[e] (nm)
1	1	1	18.3	18.2	18.3	0.17	0
2	2	2	9.3	8.3	10.2	0.11	0
3	4	3	7.9	6.9	7.9	0.18	0
4	3	4	7.8	7.6	7.8	0.12	0
5	6	5	6.6	4.9	7.2	0.11	0.1
6	5	6	5.1	4.6	6.1	0.14	0
7	7	7	4.3	3.7	5.2	0.19	0
8	9	8	4.1	3.3	4.8	0.14	0
9	8	10	3.5	3.5	3.5	0.09	0
10	10	11	3.1	3.1	3.1	0.13	0
11	11	9	2.7	2.4	4.6	0.11	0.12
12	12	12	2.3	2.2	2.4	0.16	0
13	16	14	1.8	1.7	1.9	0.13	0
14	15	15	1.8	1.8	1.7	0.1	0
15	19	16	1.6	0.8	1.7	0	0

[a] Clusters obtained using the Gromos algorithm, with backbone RMSDs as the metrics and a cutoff of 0.3 nm;

[b] Clusters obtained using the QT algorithm implemented by VMD, with backbone RMSDs as the metrics and a cutoff of 0.3 nm, listed in correspondence to the Gromos clusters;

[c] Clusters obtained using the SL algorithm, with backbone RMSDs as the metrics and a cutoff of 0.3 nm, listed in correspondence to the Gromos clusters;

[d] Backbone RMSDs between the corresponding cluster center structures obtained from the Gromos and QT algorithms.

[e] Backbone RMSDs between the corresponding cluster center structures obtained from the Gromos and SL algorithms.

Reference:

[1] F. Delaglio, S. Grzesiek, G. W. Vuister, G. Zhu, J. Pfeifer, A. Bax, *J. Biomol. NMR* **1995**, *6*, 277-293.

[2] J. A. Marsh, V. K. Singh, Z. Jia, J. D. Forman-Kay, *Protein Sci.* **2006**, *15*, 2795-2804.

[3] S. Preus, S. L. Noer, L. L. Hildebrandt, D. Gudnason, V. Birkedal, *Nat. Methods* **2015**, *12*, 593-594.

[4] Y. T. Feng, L. Zhang, S. W. Wu, Z. J. Liu, X. Gao, X. Zhang, M. L. Liu, J. W. Liu, X. H. Huang, W. N. Wang, *Angew. Chem.-Int. Edit.* **2016**, *55*, 13990-13994.

[5] a) S. Sindbert, S. Kalinin, H. Nguyen, A. Kienzler, L. Clima, W. Bannwarth, B. Appel, S. Muller, C. A. Seidel, *J Am Chem Soc* **2011**, *133*, 2463-2480; b) K. Walczewska-Szewc, B. Corry, *Phys Chem Chem Phys* **2014**, *16*, 12317-12326.

[6] J. W. van de Meent, J. E. Bronson, C. H. Wiggins, R. L. Gonzalez, Jr., *Biophys J* **2014**, *106*, 1327-1337.

[7] I. Gopich, A. Szabo, *J Chem Phys* **2005**, *122*, 14707.

[8] aY. Sugita, Y. Okamoto, *Chem. Phys. Lett.* **1999**, *314*, 141-151; bU. H. E. Hansmann, Y. Okamoto, *J. Comput. Chem.* **1993**, *14*, 1333-1338; cU. H. E. Hansmann, *Chem. Phys. Lett.* **1997**, *281*, 140-150.

[9] aY. Zhang, *BMC Bioinformatics* **2008**, *9*, 40; bA. Roy, A. Kucukural, Y. Zhang, *Nat. Protoc.* **2010**, *5*, 725-738.

[10] D. Xu, Y. Zhang, *Proteins* **2012**, *80*, 1715-1735.

[11] B. Hess, C. Kutzner, D. van der Spoel, E. Lindahl, *J. Chem. Theor. Comput.* **2008**, *4*, 435-447.

[12] P. Bjelkmar, P. Larsson, M. A. Cuendet, B. Hess, E. Lindahl, *J. Chem. Theor. Comput.* **2010**, *6*, 459-466.

[13] G. Bussi, D. Donadio, M. Parrinello, *J. Chem. Phys.* **2007**, *126*, 7.

[14] M. Parrinello, A. Rahman, *J. Appl. Phys.* **1981**, *52*, 7182-7190.

[15] T. Darden, D. York, L. Pedersen, *J. Chem. Phys.* **1993**, *98*, 10089-10092.

[16] B. Hess, H. Bekker, H. J. C. Berendsen, J. Fraaije, *J. Comput. Chem.* **1997**, *18*, 1463-1472.

[17] A. Patriksson, D. van der Spoel, *Phys. Chem. Chem. Phys.* **2008**, *10*, 2073-2077.

[18] X. Daura, K. Gademann, B. Jaun, D. Seebach, W. F. van Gunsteren, A. E. Mark, *Angew. Chem.-Int. Edit.* **1999**, *38*, 236-240.

[19] G. C. P. van Zundert, J. Rodrigues, M. Trellet, C. Schmitz, P. L. Kastritis, E. Karaca, A. S. J. Melquiond, M. van Dijk, S. J. de Vries, A. Bonvin, *J. Mol. Biol.* **2016**, *428*, 720-725.

[20] S. N. Mattagajasingh, S. C. Huang, E. J. Benz Jr, *Clin. Transl. Sci.* **2009**, *2*, 102-111.

[21] W. Kabsch, C. Sander, *Biopolymers* **1983**, *22*, 2577-2637.

[22] B. Han, Y. F. Liu, S. W. Ginzinger, D. S. Wishart, *J. Biolmol. NMR* **2011**, *50*, 43-57.

[23] P. Romero, Z. Obradovic, X. H. Li, E. C. Garner, C. J. Brown, A. K. Dunker, *Proteins* **2001**, *42*, 38-48.